Journal of Alloys and Compounds 504 (2010) 83–88

Contents lists available at ScienceDirect

Journal of Alloys and Compounds

journal homepage: www.elsevier.com/locate/jallcom

The effect of high-pressure torsion on the microstructure and hydrogen absorption kinetics of ball-milled $Mg_{70}Ni_{30}$

Á. Révész[a,*], Zs. Kánya[a], T. Verebélyi[a], P.J. Szabó[b], A.P. Zhilyaev[c,d], T. Spassov[e]

[a] Department of Materials Physics, Eötvös University, P.O.B. 32, H-1518 Budapest, Hungary
[b] Department of Materials Science and Engineering, University of Technology and Economy, H-1111 Budapest, Hungary
[c] Centro Nacional de Investigaciones Metalúrgicas, 28040 Madrid, Spain
[d] Institute for Metals Superplasticity Problems, RAS, 450001 Ufa, Russia
[e] Department of Chemistry, University of Sofia "St. Kl. Ohridski", 1 J. Bourchier str., 1164 Sofia, Bulgaria

ARTICLE INFO

Article history:
Received 29 March 2010
Received in revised form 6 May 2010
Accepted 7 May 2010
Available online 20 May 2010

Keywords:
Nanostructure
Ball milling
Deformation
Hydrogen storage
X-ray diffraction

ABSTRACT

Ball-milled nanocrystalline $Mg_{70}Ni_{30}$ powders were subjected to heavy shear deformation by the process of high-pressure torsion (HPT). X-ray diffraction analysis revealed that HPT results in a deformation-dependent microstructural refinement. Complementary hydrogen sorption kinetic measurements indicate that the maximum absorption capacity is increased by 30–50% after HPT due to the creation of new possible hydrogen absorption sites at the grain boundaries and at lattice defects.

1. Introduction

Hydrogen as the most abundant element in the world can serve as a promising energy carrier in the near future. In order to commercialize the hydrogen energy, production, transmission and usage must achieve a threshold of efficiency. Storing hydrogen in the solid state remains a significant technological challenge that must be solved if hydrogen is to be applied as a fuel [1]. Recently novel approaches to reach hydrogen based energy systems resulted in a great interest to metal/intermetallic hydride storage solutions. Magnesium is considered as one of the most attractive hydrogen storage materials, mainly because of high-storage capacity (7.6 wt.%), lightweight and low cost [2]. Nevertheless, high thermodynamic stability ($\Delta H = -75$ kJ/mol) [3], high hydrogen desorption temperature (higher than 400 °C) and relatively poor hydrogen absorption–desorption kinetics at temperatures below 350 °C impedes the use of Mg in industrial applications. To improve the hydrogen storage properties of magnesium, nanosized Mg powders have been produced by mechanical alloying [4–6]. Ball milling (BM) of Mg/MgH_2 up to several hours results in fine nanopowder with a typical average grain size ranging from 10 to 30 nm [7–10]. By reducing the grain size to nanocrystalline dimensions, the H-sorption kinetics are accelerated substantially due to the increased volume fraction of grain boundaries, and the hydrogen desorption temperature is decreased by about 100 °C [10–12].

Among Mg-based alloys, binary Mg–Ni is the most remarkable due to its favorable thermodynamics [13]. In this system there exhibit two intermetallic line compounds, i.e. Mg_2Ni and $MgNi_2$, however, from the standpoint of hydrogen storage only the former possesses significant gravimetric hydrogen capacity of 3.62 wt.% [14]. BM of Mg + Ni powders from elemental powders results in impressive improvement of the hydrogen sorption kinetics [15–17]. It has recently been found that the static value of absorbed hydrogen under isothermal conditions of BM-Mg_2Ni can further be improved during a dynamic milling process due to local structural changes and temperature rise [18,19]. The mechanical alloying of the mixture of $Mg_2Ni + MgNi_2$ results in nanocrystallization and some solid-state amorphization of hexagonal Mg_2Ni, however, $MgNi_2$ is resistant to nanostructurization [20]. The addition of only 0.5 mol% Ni to nanocrystalline MgH_2 results in considerable decrease of the dehydrogenation temperature [21].

Up to now, besides BM a variety of other methods have been applied to improve the hydriding properties of Mg-based alloys. The production of Mg_2Ni by hydrogen combustion synthesis results in a maximum capacity of 2.76 wt.% within 100 s at 313 K [22] which can further be increased above 5 wt.% by adding metal

* Corresponding author. Tel.: +36 1 372 2823; fax: +36 1 372 2811.
E-mail address: reveszadam@ludens.elte.hu (Á. Révész).

0925-8388/$ – see front matter © 2010 Elsevier B.V. All rights reserved.
doi:10.1016/j.jallcom.2010.05.058

oxide catalyst [23]. The sorption kinetics of liquid cast hypoeutectic Mg–Mg_2Ni alloy system has shown no sign of reduced capacity over 200 cycles [24]. Improved hydrogen storage capacity and kinetics can be achieved on bulky Mg-based samples by different techniques based on severe plastic deformation, such as equal channel angular pressing [25,26] and high-pressure torsion (HPT) [27]. These techniques originally were invented for producing porosity and impurity-free bulk nanocrystalline samples with high strength and relatively good ductility [28–31].

In this paper the consequent application of BM and HPT on $Mg_{70}Ni_{30}$ powders will be demonstrated. The effect of microstructure on the hydrogen storage properties will also be discussed.

2. Experimental

2.1. Powder processing

Ball milling blends of commercial polycrystalline Mg and Ni powders (supplied by Sigma–Aldrich) with a purity of 99.9% was carried out using a SPEX 8000 Mixer Mill for different durations ranging from 1 to 10 h. It is a high-energy shaker mill that swings the hardened steel cylindrical milling vial (inside diameter 38 mm and length 57 mm) in a complex three-dimensional pattern. The main component of the vial motion is a vibration with a frequency of 17.6 Hz, approximate amplitude of 25.6 mm, and a maximum velocity of about 2.8 m/s.

In order to ensure an approximately uniform distribution of impacts, the container was filled with $10\frac{1}{4}''$ balls, made of hardened steel with a 10:1 ball to powder weight ratio. The powders were always filled into the milling container in an argon-flushed glove box.

2.2. High-pressure torsion

Some portion of the powders milled for 1 and 10 h were placed between anvils of a high-pressure torsion device and then compressed and deformed into disks with a radius of $R = 5$ and thickness of $L = 200$ μm, under an applied pressure of 6 GPa with $N = 5$ whole turns. Further details of HPT processing are given elsewhere [28,29]. The accumulated shear strain for torsion deformation at a radius r at time t can be represented by:

$$\varepsilon(r, t) = \frac{\omega t r}{L}, \quad (1)$$

where $\omega = 2\pi$/min is the angular speed of rotation. In order to investigate the deformation dependence of the microstructure and thermal behavior, the HPT disks were fragmented into small pieces, and systematically sorted into three groups according to their distance from the centre. Hereafter these selections will be denoted as sectors A, B and C with equidistant radius from the torsion axis.

2.3. Microstructural characterization

Morphology studies on the ball-milled powders were performed on a Philips XL 30 scanning electron microscopy (SEM) in backscattered electron (BSE) mode. The compositional changes of the surface related directly to contrast differences in the BSE image were revealed and quantitatively determined by energy dispersive X-ray (EDX) analysis with a relative accuracy of 3%.

The evolution of the microstructure during absorption/desorption cycles was monitored by X-ray powder diffraction (XRD) with Cu-K_α radiation on a Philips X'pert powder diffractometer in θ–2θ geometry and was characterized by X-ray line profile analysis. The instrumental pattern was measured on a NIST SRM660a LaB_6 peak profile standard material.

Local area X-ray diffraction (XRD) measurements were carried out on a high-resolution double crystal diffractometer with negligible instrumental broadening equipped with a fine focus rotating copper anode (Nonius, FR 591) operating at 45 kV and 80 mA. The symmetrical Ge (220) primary monochromator produced monochromatic Cu-K_α radiation. The spot size of the X-ray beam on the specimen was 100 μm × 500 μm. Diffraction patterns were registered by FUJI Imaging Plate (BAS MS2025). The average crystallite size $\langle D \rangle$ was determined by applying the Williamson–Hall technique [32] after deconvolution and fitting the Bragg-peaks by pseudo-Voight function. The usual error of $\langle D \rangle$ is about 10%.

2.4. Thermal characterization

A Perkin Elmer power compensated differential scanning calorimeter (DSC) was used to investigate the thermal behavior applying continuous heating experiments performed at scan rate of 40 K/min. All measurements were carried out under argon atmosphere. The temperature and the enthalpy were calibrated using pure In and Al. Each measurement was followed by a second run in order to obtain the baseline.

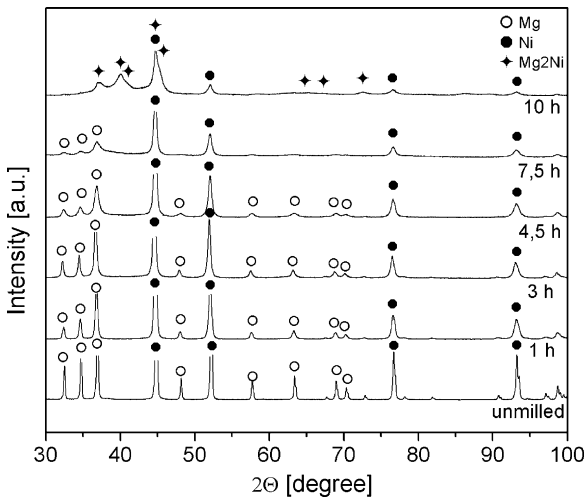

Fig. 1. XRD patterns of $Mg_{70}Ni_{30}$ powders ball-milled for different times.

2.5. Hydrogen sorption kinetics

The pressure–composition isotherms and H-sorption kinetics were measured by a Sieverts'-type apparatus (PCT) at 573 K, under hydrogen pressure of 12 bar during absorption and under 0.5 bar during desorption. The first measurement is considered as the activation of the surface passivation layer, therefore the subsequent experiment was used for quantitative analysis.

3. Results and discussion

3.1. Characterization of ball-milled $Mg_{70}Ni_{30}$ powders

A general view on the effect of milling on the microstructure of BM-$Mg_{70}Ni_{30}$ powder blend can be inferred from Fig. 1. The diffractogram of the as-received powder is characterized by the Bragg-peaks of hexagonal Mg (JCPDS 35-0821) and fcc Ni (JCPDS 45-1027). As the milling is introduced the diffraction peaks become significantly broader indicating grain-size refinement and/or lattice strain generated by the attrition. The relative intensity of the Mg-peaks continuously decreases, however Mg is still present in the powder milled for 7.5 h. Longer milling up to 10 h results in an abrupt change of the XRD pattern, incorporating the presence of stochiometric hexagonal Mg_2Ni line compound (JCPDS 35-1225) accompanied with a very faint amorphous halo centered at around 42°. At this point no traces of Mg is present, however, Ni still dominates the pattern. Although the composition of the as-received powder blend is in excess of Mg compared to the stochiometric concentration, the presence of residual Ni can be attributed to the different mechanical properties of the two components. The excess Mg most probably covers the inner surfaces of the milling media, or promotes a minor amorphous phase suggested by Guzman et al. [33].

The evolution of the average grain size obtained by the Williamson–Hall analysis is plotted in Fig. 2. A usual tendency is confirmed, i.e. both Mg and Ni achieve nanometric dimensions with final grain sizes of $\langle D \rangle = 13$ nm and $\langle D \rangle = 30$ nm, respectively, in correlation with literature data [34]. The faster microstructural refinement of Mg compared to Ni results in Mg-enriched grain boundaries compared to the grain interiors coupled with increased reactivity to produce the amorphous phase [33,35]. The average grain size of the Mg_2Ni compound phase achieved from thermal and/or mechanical transformation of the amorphous phase is about $\langle D \rangle = 11$ nm [33].

SEM photographs taken from some selected powder blends (Fig. 3) complete some certain aspects of the XRD patterns. After 1 h of milling the powder is characterized by flat particles with

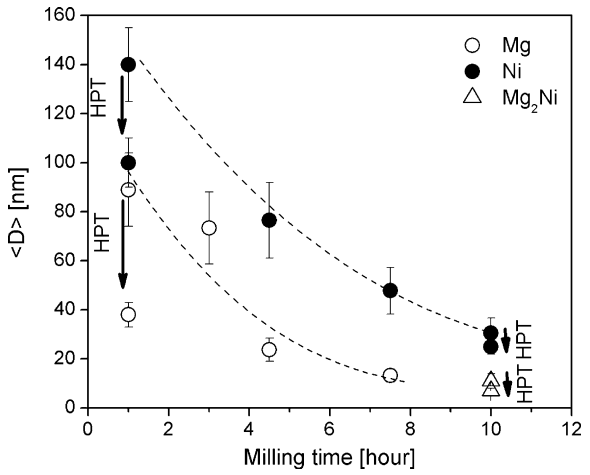

Fig. 2. Variation of the average grain size ⟨*D*⟩ during the milling process obtained for Mg, Ni and Mg_2Ni phases. The arrows denote the change of ⟨*D*⟩ due to the extreme shear deformation generated by HPT.

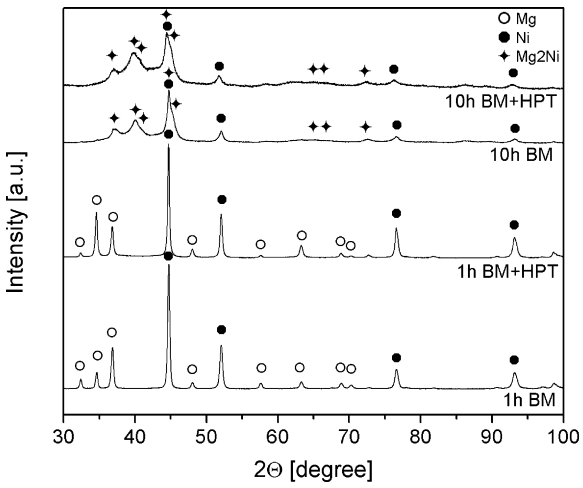

Fig. 4. XRD patterns of $Mg_{70}Ni_{30}$ powders and HPT disks.

sharp edges of considerable different size (see Fig. 3a). As seen, the individual particles are intact and compact, lacking any visible cracks, which are responsible for enhanced hydrogen diffusion. The surface is flat, only some minor contamination can act as a hydrogen chemisorption place. The corresponding particle size histogram obeys log-normal distribution with a median of $m = 80 \pm 5$ μm and variance $\sigma = 0.47$, similarly to the work of Milanese et al. [36]. As seen in Fig. 3b the $Mg_{70}Ni_{30}$ powder milled for 10 h is characterized by smaller particles. These particles are considerably attrited, forming larger agglomerates and dominated by cracks and paths. The corresponding particle size histogram can well be fitted by log-normal function (Fig. 3b) with $m = 7 \pm 1$ μm and $\sigma = 0.46$. The obtained decrease of the average particle size of Mg_2Ni below literature values [35] is a consequence of the special parameters of the SPEX mill. This refined structure both on micron and nanoscale is more favorable for the chemisorption of H_2 and evidently the required hydrogen diffusion length during a sorption process is much shorter [37]. Quantitative EDX analysis confirmed that average concentration of the powder ($Mg_{65}Ni_{35}$) is enriched in Ni, in accordance with the XRD pattern (see Fig. 1).

3.2. The effect of high-pressure torsion

Based on preliminary experiments, we have chosen two powder samples (milled for 1 and 10 h) for further processing by HPT. The corresponding powder diffractograms averaging the scattering from the whole disks indicate some progress compared to those of the as-milled powders (Fig. 4). The XRD pattern of the sample milled for 1 h and deformed by HPT (1 h BM + HPT) exhibits some line broadening accompanied with the refinement of the average grain size down to 38 and 100 nm for Mg and Ni, respectively

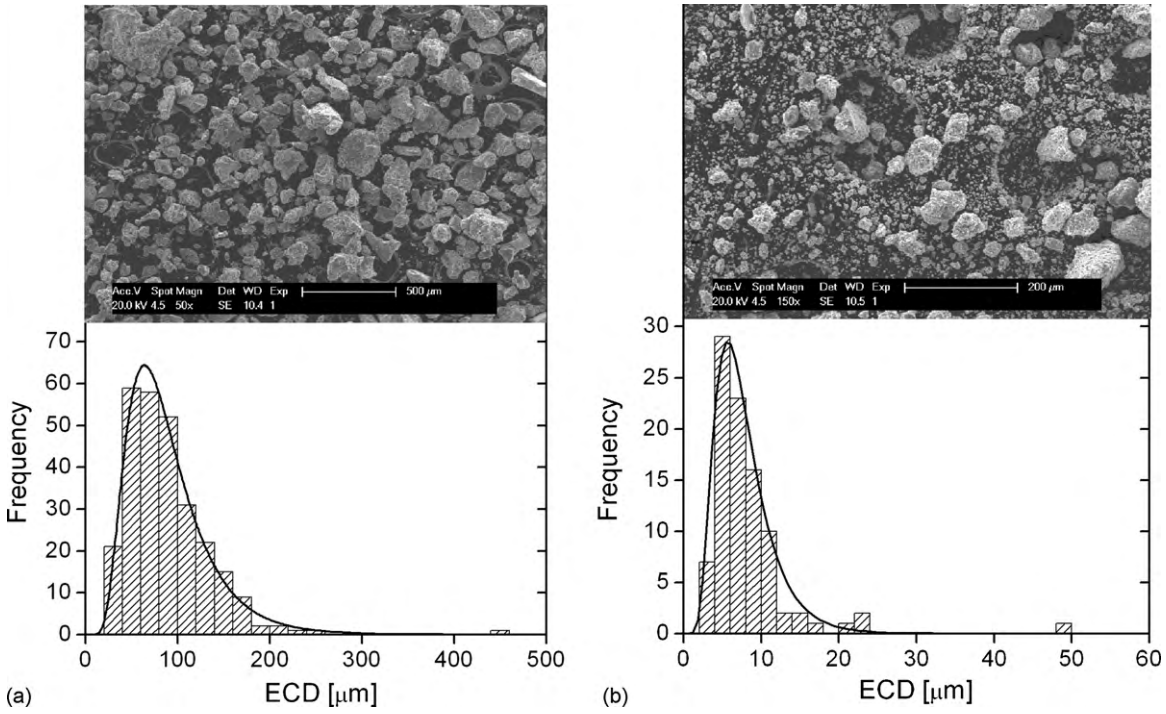

Fig. 3. SEM image and the corresponding particle size histogram of $Mg_{70}Ni_{30}$ powders milled for (a) 1 h and (b) 10 h. Quantitative EDX analysis confirmed that average concentration of the powder is $Mg_{65}Ni_{35}$.

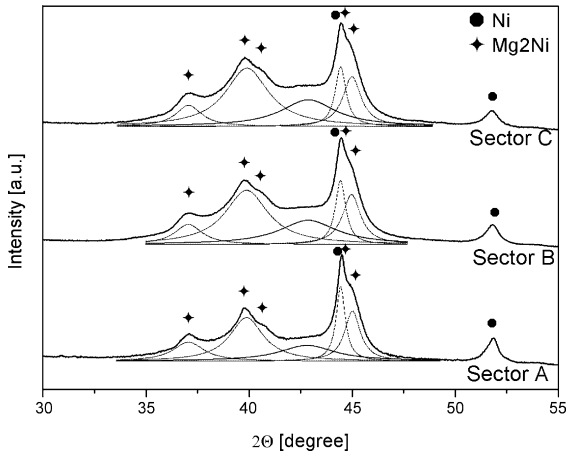

Fig. 5. Local area XRD measurements taken at different positions on the surface of the HPT disk processed by BM for 10 h and subsequent torsion $N = 5$ revolutions under 6 GPa at a speed of 1 rev/min.

(see Fig. 2). As an effect of uniaxial compression and simultaneous shear deformation, the relative intensities of the Mg-peaks changes considerably, i.e. from $I(1\,0\,1)/I(0\,0\,2) = 2.5$ to $I(1\,0\,1)/I(0\,0\,2) = 0.8$, indicating the development of anisotropy [27]. As also seen, the HPT does not promote intermetallic formation. The disk processed by BM for 10 h and subsequent torsion (10 h BM + HPT) exhibits similar microstructure as the as-milled powder, i.e. the dominant phase is the Mg_2Ni compound ($\langle D\rangle = 7$ nm), while residual Ni is also present ($\langle D\rangle = 25$ nm). Minor differences can be observed in the increased background which is most probably connected to some additional amorphization in the solid state. Such (partial) amorphization is observed during plastic deformation of multicomponent metallic alloys during HPT [38–41].

In order to reveal the deformation dependence (see Eq. (1)) of the microstructure, local area X-ray diffractograms were taken on different sectors of the 10 h BM + HPT disk (Fig. 5). The high-resolution patterns presenting peak deconvolution obeys some deformation dependence, i.e. the Ni-peak intensities marginally decrease while the contribution of the amorphous halo increases with increasing deformation. The relative magnitude of the amorphous halo is larger by almost a factor of two for sector C than for sector A, in line with a more efficient solid-state amorphization with increasing deformation [39]. The obtained average $\langle D\rangle$ grain-size values for Mg_2Ni and Ni indicates that larger shear deformation at the perimeter of the disk results in further refinement (Fig. 6).

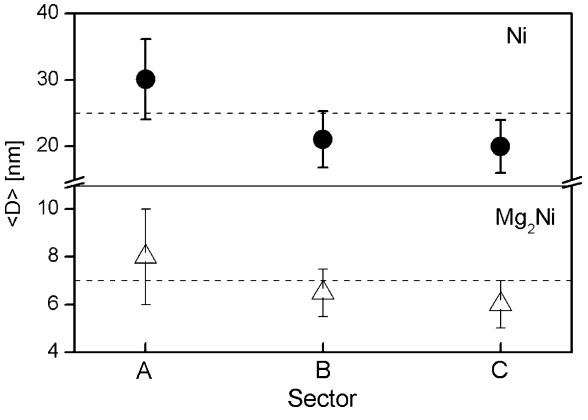

Fig. 6. Variation of grain size $\langle D\rangle$ for Mg_2Ni and Ni as a function of deformation in the case of the HPT disk processed by BM for 10 h and subsequent torsion obtained from local area X-ray diffraction. Dashed lines indicates the values averaged for the whole disk obtained from powder diffraction.

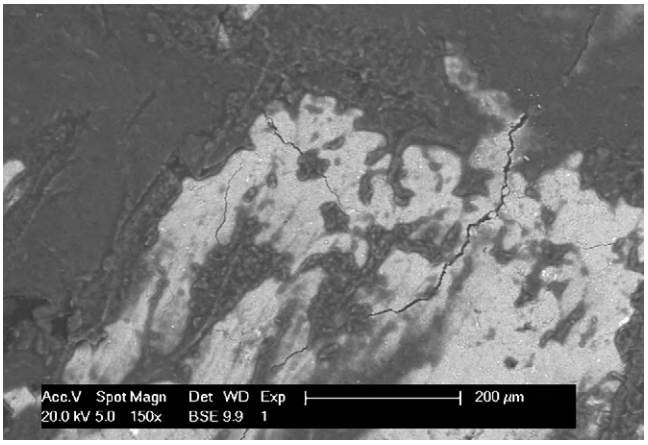

Fig. 7. SEM image taken on the cross section of the HPT disk processed by BM for 10 h and subsequent torsion.

The SEM BSE image obtained on the polished cross section of the 10 h BM + HPT disk is shown in Fig. 7. Note that due to the extreme deformation, the original morphology has undergone drastic changes, i.e. the individual powder particles cannot be distinguished corresponding to an efficient compaction. Generally, the specimen is brittle, open cracks parallel to the sample surface are visible. Close to the torsion axis (sector A) some large blocks with an average diameter of 500 μm are present. Quantitative EDX analysis confirmed that these blocks are enriched in Ni ($Mg_{62}Ni_{38}$), while the dark background has a composition of $Mg_{70}Ni_{30}$ containing mainly the Mg_2Ni compound phase.

The thermal stability of the disks was systematically analysed by calorimetry. Continuous heating DSC curves corresponding to the different sectors of the 1 h BM + HPT disk obtained at a heating rate of 40 K min^{-1} are plotted in Fig. 8. As seen, each curve presents two exothermic calorimetric peaks (T_1 and T_2) indicating a two stage thermal event, similarly to the ball-milled Mg_2Ni powder [33]. Transformation enthalpies (ΔH_1, ΔH_2) were obtained as the area of the first and second exothermic peak, respectively. The monotonous increase of ΔH_1, ΔH_2 and $\Delta H_{tot} = \Delta H_1 + \Delta H_2$ is related to a more metastable state with increasing strain (see the inset in Fig. 8). In order to reveal the T_1 and T_2 thermal events, continuous heating scans of the most deformed part (sector C) were taken up to 460 and 660 K. As the diffractogram indicates, dur-

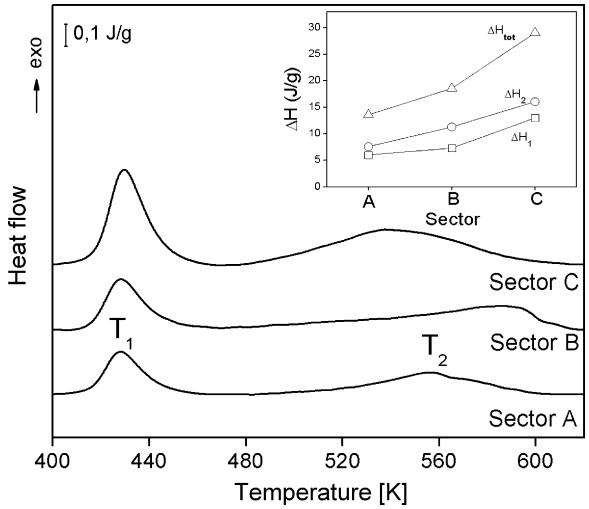

Fig. 8. Linear heating DSC scans corresponding to different sectors of the $Mg_{70}Ni_{30}$ HPT disk processed by BM for 1 h and subsequent torsion.

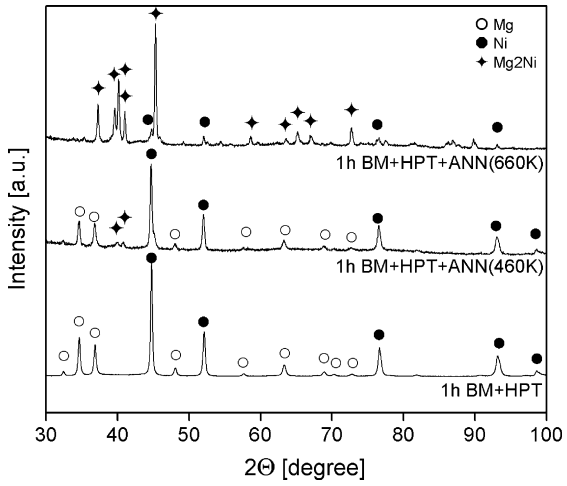

Fig. 9. XRD patterns corresponding to the heat treatments at 460 and 660 K of the most deformed part (sector C) of the 1 h BM + HPT disk.

ing the T_1 thermal event only narrowing of the Bragg-peaks occurs (Fig. 9), resulting in a final grain size of $\langle D \rangle$ = 59 nm and $\langle D \rangle$ = 127 nm for Mg and Ni, respectively. The subsequent T_2 transformation promotes the nucleation of the Mg_2Ni compound phase at the expense of Mg and Ni, in accordance with the equilibrium phase diagram. The T_2 temperature characterizing the Mg + Ni → Mg_2Ni is considerably higher than for BM-Mg_2Ni [34] due to the increased thermal stability induced by the severe shear deformation.

3.3. Hydrogen absorption properties

Hydriding kinetic data for the nanocrystalline $Mg_{70}Ni_{30}$ powders milled for 1 and 10 h as well as for the shear-deformed disk obtained at 573 K are presented in Fig. 10a and b. The as-milled powders and the HPT samples absorb hydrogen almost without activation, as the maximum capacity is reached after the first couple of absorption–desorption cycles. The maximum capacity of the powders is about 2 and 2.4 wt.% obtained after BM for 1 and 10 h, respectively (see Table 1). The larger value corresponding to longer BM time is a consequence of the finer structure both on micron and nanoscale (see Figs. 2 and 3a and b), in accordance with previous findings [37].

Noticeably improvement in the H-uptake is observed when the powders are subjected to the HPT deformation. The obtained capacity of 3 wt.% corresponds to the composition of $Mg_2NiH_{3.3}$ and means nearly complete hydriding. On one hand, this increase can be attributed to the smaller crystallite size, i.e. to the enhanced specific surface area, on the other hand intense straining [28] and/or lattice defects (e.g. dislocations) generated during the heavy shear deformation can also act as possible hydrogen absorption sites in the grain interiors by enhancing the diffusion of the H atoms. Although, the two disks exhibit considerably different average grain size as well as different dominant crystallographic phases (see Fig. 2), the practically similar final H-storage value indicates that the abundant lattice defects have a crucial role in the creation of new and easy accessible hydrogen sites. Horita and co-workers found that a noticeable hydrogen storage performance can be achieved in coarse-grained $MgNi_2$ by HPT due to the intense anisotropic strain [27], although this compound possesses no measurable capacity under equilibrium conditions [14].

In general, the initial absorption kinetics is fast for all samples, reaching about 50% of hydriding within the first 500–600 s. The initial absorption rate obtained from the slope of the fitted straight line on the sorption curves in the range of 100–500 s indicates a moderate decrease due to HPT for both the 1 and 10 h alloy (see Table 1).

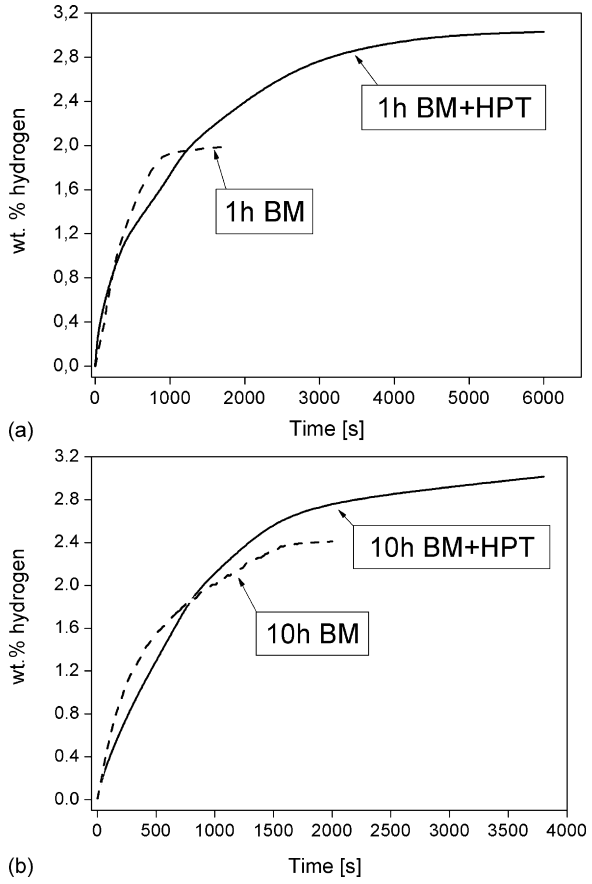

Fig. 10. Hydrogen kinetic absorption curves of $Mg_{70}Ni_{30}$ powder milled for 1 h and then processed by HPT (a) and powder milled for 10 h and then deformed by HPT (b).

Table 1
Maximum capacity and initial absorption rate of BM-$Mg_{70}Ni_{30}$ powders and HPT disks.

Sample	Capacity (wt.%)	Absorption rate ($\times 10^{-3}$ wt.%/s)
1 h BM	2.0	3.2
1 h BM + HPT	3.0	2.4
10 h BM	2.4	5.3
10 h BM + HPT	3.0	3.0

This phenomenon can be related to the simultaneous compaction and shear which affects the (sub)grain structure of the specimens (compare Figs. 7 and 3a and b), hindering the fast diffusion of the hydrogen atoms along the denser grain boundaries. However, during the subsequent stage of the process (beyond 800–1000 s), the absorption is much faster in the case of the HPT samples due to the increased number of lattice defects.

4. Conclusions

Ball milling of $Mg_{70}Ni_{30}$ powders results in a gradual microstructural refinement accompanied with a Mg + Ni → Mg_2Ni reaction at prolonged milling times. Coupled X-ray diffraction and EDX analysis confirmed that average concentration of all the BM powders is enriched in Ni. Subsequent, simultaneous compaction and shearing of the powders into disks by high-pressure torsion results in a microstructural refinement accompanied with the creation of straining and/or lattice defects. Local area XRD experiments have shown that the decrease of the average crystallite size is more pronounced at the perimeter of the disks in accordance with a larger enthalpy release detected by calorimetry. Absorption kinetic data

indicate that the maximum H-absorption capacity is increased by 30–50% after HPT due to the creation of new possible hydrogen absorption sites at the grain boundaries and at lattice defects. On the other hand, the initial absorption rate is somewhat decreased due to HPT.

Acknowledgements

We appreciate the support of the Hungarian Scientific Research Fund under grant No. F67893 and of the Bulgarian National Science Fund under grant DO 02-226/2008. Á. R. is indebted for the János Bolyai Research Scholarship of the Hungarian Academy of Sciences.

References

[1] R.A. Varin, T. Czujko, Z.S. Wronski, Nanomaterials for Solid State Hydrogen Storage, Springer Science, New York, 2009.
[2] R.C. Bowman, B. Fultz, Mater. Res. Bull. 27 (2002) 688.
[3] K.H.J. Buschow, P.C.P. Bouten, A.R. Miedema, Rep. Prog. Phys. 46 (1982) 937.
[4] R.A. Varin, T. Czujko, Ch. Chiu, Z. Wronski, J. Alloys Compd. 424 (2006) 356.
[5] L. Zaluski, A. Zaluska, P. Tessier, J.O. Ström-Olsen, R. Schulz, Mater. Sci. Forum 225 (1996) 853.
[6] G. Liang, S. Boily, J. Huot, A. Van Neste, R. Schulz, J. Alloys Compd. 276 (1998) 302.
[7] M. Danaie, D. Mitlin, J. Alloys Compd. 476 (2008) 590.
[8] M. Porcu, A.K. Petford-Long, J.M. Sykes, J. Alloys Compd. 453 (2008) 341.
[9] V. Fuster, G. Urretavizcaya, F.J. Castro, J. Alloys Compd. 481 (2009) 673.
[10] D. Fátay, Á. Révész, T. Spassov, J. Alloys Compd. 399 (2005) 237.
[11] W. Oelerich, T. Klassen, R. Bormann, J. Alloys Compd. 315 (2001) 237.
[12] G. Barkhordarian, T. Klassen, R. Borman, J. Alloys Compd. 364 (2004) 242.
[13] K. Zeng, T. Klassen, W. Oelerich, R. Bormann, J. Alloys Compd. 283 (1999) 213.
[14] J.J. Reilly, R.H. Wiswal, Inorg. Chem. 7 (1968) 2254.
[15] A. Zaluska, L. Zaluski, J.O. Ström-Olsen, Appl. Phys. A 72 (2001) 157.
[16] S. Orimo, H. Fuji, Appl. Phys. A 72 (2001) 167.
[17] C.A. Chung, Ci-Siang Lin, Int. J. Hydrogen Energy 34 (2009) 5429.
[18] G. Mulas, F. Delogu, G. Cocco, J. Alloys Compd. 473 (2009) 180.
[19] F. Delogu, G. Mulas, Int. J. Hydrogen Energy 34 (2009) 3026.
[20] R.A. Varin, T. Czujko, J. Mizera, J. Alloys Compd. 350 (2003) 332.
[21] H. Simchi, A. Kaflou, A. Simchi, Int. J. Hydrogen Energy 34 (2009) 7724.
[22] X. Liu, Y. Zhu, L. Li, J. Alloys Compd. 455 (2008) 197.
[23] H. Gu, Y. Zhu, L. Li, Int. J. Hydrogen Energy 34 (2009) 7707.
[24] K. Nogita, S. Ockert, J. Pierce, M.C. Greaves, C.M. Gourlay, A.K. Dahle, Int. J. Hydrogen Energy 34 (2009) 7686.
[25] V.M. Skripnyuk, E. Rabkin, Y. Estrin, R. Lapovok, Acta Mater. 52 (2004) 405.
[26] V.M. Skripnyuk, E. Rabkin, Y. Estrin, R. Lapovok, Int. J. Hydrogen Energy 34 (2009) 6320.
[27] Y. Kusadome, K. Ikeda, Y. Nakamori, S. Orimo, Z. Horita, Scripta Mater. 57 (2007) 751.
[28] R.Z. Valiev, R.K. Ishlamgaliev, I.V. Alexandrov, Prog. Mater. Sci. 45 (2000) 103.
[29] A.P. Zhilyaev, T.G. Langdon, Prog. Mater. Sci. 53 (2008) 893.
[30] A.P. Zhilyaev, B.K. Kim, G.V. Nurislamova, M.D. Baro, J.A. Szpunar, T.G. Langdon, Scripta Mater. 46 (2002) 575.
[31] T. Hebesberger, H.P. Stüwe, A. Vorhauer, F. Wetscher, R. Pippan, Acta Mater. 53 (2005) 393.
[32] G.K. Williamson, W.H. Hall, Acta Metall. 1 (1953) 22.
[33] D. Guzman, S. Ordonez, J.F. Fernandez, C. Sanchez, D. Serafini, P.A. Rojas, C. Aguilar, Int. J. Hydrogen Energy 34 (2009) 5429.
[34] F.C. Gennari, M.R. Esquivel, J. Alloys Compd. 459 (2008) 425.
[35] P. Rojas, S. Ordonez, D. Serafini, A. Zuniga, E. Lavernia, J. Alloys Compd. 391 (2005) 267.
[36] C. Milanese, A. Girella, S. Garroni, G. Bruni, V. Berbenni, P. Matteazzi, A. Marini, Int. J. Hydrogen Energy 35 (2010) 1285.
[37] Á. Révész, D. Fátay, T. Spassov, J. Alloys Compd. 434–435 (2007) 725.
[38] A.V. Sergueeva, C. Song, R.Z. Valiev, A.K. Mukherjee, Mater. Sci. Eng. A 339 (2003) 159.
[39] Á. Révész, J.L. Lábár, S. Hóbor, A.P. Zhilyaev, Zs. Kovács, J. Appl. Phys. 100 (2006) 103522.
[40] Zs. Kovács, S. Hóbor, P.J. Szabó, J. Lendvai, A.P. Zhilyaev, Á. Révész, Mater. Sci. Eng. A 449–451 (2007) 1139.
[41] Y.F. Sun, T. Nakamura, Y. Todaka, M. Umemoto, N. Tsuji, Intermetallics 17 (2009) 256.